Extracting the Dominant SST Modes Impacting North America's Observed Climate*

FUYAO WANG

Nelson Institute Center for Climatic Research, University of Wisconsin—Madison, Madison, Wisconsin

ZHENGYU LIU

Laboratory of Climate, Ocean–Atmosphere Studies, Peking University, Beijing, China, and Nelson Institute Center for Climatic Research, University of Wisconsin—Madison, Madison, Wisconsin

MICHAEL NOTARO

Nelson Institute Center for Climatic Research, University of Wisconsin—Madison, Madison, Wisconsin

(Manuscript received 1 August 2012, in final form 16 December 2012)

ABSTRACT

The seasonal impacts of the dominant sea surface temperature (SST) modes to North American climate are assessed comprehensively in observations using the multivariate generalized equilibrium feedback assessment (GEFA) method. The GEFA method is first validated before applying it to observations. Impacts of each individual SST mode are quantified and the associated mechanisms are discussed. Four critical SST modes for North American climate are found: the ENSO mode, Indian Ocean Basin (IOB) mode, North Pacific first empirical orthogonal function (EOF) mode, and tropical Atlantic second EOF mode. The impacts of the ENSO mode are consistent with previous studies qualitatively, while the impact strength is further quantified here. The IOB mode has a strong influence on surface air temperature across North America, and it is demonstrated for the first time that its impact strength might even exceed that of ENSO during both winter and summer. The IOB mode also affects the year-round precipitation. A deeper understanding of the impact of North Pacific SSTs on wintertime surface air temperature is achieved: namely, positive SST anomalies in the Kuroshio Extension region correspond to colder (warmer) air in western (eastern) North America. The tropical Atlantic has a more significant influence on North American precipitation than does the extratropical Atlantic, with colder than normal tropical North Atlantic SSTs supporting wetter conditions across much of the United States, especially during autumn. Because of the linearity of GEFA, the total impacts of multiple SST modes can be obtained by the linear combination of each individual mode's impact. The GEFA method is a potentially powerful tool for seasonal climate prediction.

1. Introduction

In contrast with the atmosphere, the ocean is a slowly varying component of the climate system (Deser et al. 2003). This slow component makes climate predictability more feasible. Therefore, understanding the impacts of sea surface temperature (SST) on the atmosphere is critical for accurately predicting the climate state. Great efforts have been made to assess the ocean's influence on the atmosphere through individual SST modes, such as the El Niño–Southern Oscillation (ENSO) mode, Pacific decadal oscillation (PDO), Indian Ocean Basin (IOB) mode, and the Atlantic multidecadal oscillation (AMO), or combinations of modes, using either models or observations. However, model studies suffer from model deficiencies and the results vary with their dynamics and parameterization schemes. In observational studies, few works have attempted to distinguish the impact of each individual forcing in a comprehensive way. As such, the relative strengths of the impacts of different SST modes have not been well studied.

* Nelson Institute Center for Climatic Research Publication Number 1134.

Corresponding author address: Fuyao Wang, Center for Climatic Research, University of Wisconsin—Madison, 1225 West Dayton St., Madison, WI 53706.
E-mail: fwang26@wisc.edu

DOI: 10.1175/JCLI-D-12-00583.1

ENSO is considered the most prominent source of climate interannual variability, and its impact on North American climate has been recognized for decades (Ropelewski and Halpert 1986, 1987; Ting and Wang 1997; Zhang et al. 2011). In winter, past studies generally agree that, during the warm phase of ENSO, the air is warmer than normal stretching from northwestern North America to eastern Canada, colder than normal in the southern and southeastern U.S. (Ropelewski and Halpert 1986, 1987; Kiladis and Diaz 1989; Halpert and Ropelewski 1992; Zhang et al. 2011), and wetter than normal over the U.S. Southeast and Mexico (Ropelewski and Halpert 1986, 1989; Seager et al. 2005a; Zhang et al. 2011). Summertime precipitation has received greater attention, especially regarding the causes of the mega-droughts of the 1930s, 1950s, late 1980s, and 1998–2002 and pluvials of the early twentieth century and 1990s (Trenberth et al. 1988; Trenberth and Guillemot 1996; Ting and Wang 1997; Hoerling and Kumar 2003; Schubert et al. 2004; Seager et al. 2005b; Hu and Huang 2009). A linear relationship exists between precipitation over the U.S. Great Plains and ENSO with the warm (cold) phase of ENSO corresponding to wetter (drier) conditions (Trenberth and Guillemot 1996; Ting and Wang 1997).

The impact of North Pacific SST on North American climate remains inconclusive. The dominant SST modes across the North Pacific Ocean remain uncertain (Mantua et al. 1997; Schneider and Cornuelle 2005; Guan and Nigam 2009), and disagreements exist about whether its dominant SST mode has an impact on North American climate. Take PDO, a long-lived (20–30-yr persistence) El Niño–like pattern (Mantua and Hare 2002), with similar spatial climate fingerprints in the tropical Pacific to ENSO, for an example. Some studies have suggested that PDO influences North American climate. Mantua et al. (1997) and Mantua and Hare (2002) found that, during the cold season (November–April), the warm phase of observed PDO corresponds to an observed warm anomaly across northwestern North America, cold anomaly across the U.S. Southeast and Mexico, drier conditions across interior Alaska and a zone stretching from the Pacific Northwest to the Great Lakes Basin and Ohio valley, and wetter conditions in the U.S. Southwest and Mexico. Some studies, however, have concluded that PDO does not influence North American climate. Using observational data, Hu and Huang (2009) found that, in the absence of ENSO, PDO cannot significantly influence the climate of North America.

Growing evidence suggests that Indian Ocean SSTs have significant impacts on North American climate. Wu and Kinter (2009) concluded that persistent U.S. summertime droughts were favored when the tropical Indian Ocean is anomalously warm, and this relationship was particularly distinct during the second half of the twentieth century. Yang et al. (2009) investigated the relationship between the IOB index in March–May (MAM; after removed the Niño-3.4 index) and 200-hPa geopotential height in the following summer. Over North America, except Alaska, anomalous high pressure dominated during positive IOB mode. Although some studies disagree (Schubert et al. 2004), growing evidence suggests the importance of Indian Ocean SSTs to North American circulation and precipitation.

The influence of Atlantic SSTs on North American climate did not receive much attention until recently (Enfield et al. 2001). As a pioneer, Enfield et al. (2001) used the observed AMO index (defined as the 10-yr running mean of detrended Atlantic SST anomalies north of the equator; traditional AMO index) to represent the evolution of North Atlantic SSTs and found that, during the warm (cold) phase of AMO, rainfall is below (above) normal over most of the United States. Rogers and Coleman (2003) found similar results through analyzing streamflow in the upper Mississippi River. Feng et al. (2008, 2011), using proxy paleo data and multiple global climate models, confirmed the important role of AMO on North American drought. Regressing out the influence of Pacific SSTs, Guan and Nigam (2009) defined a new AMO pattern, which is a multidecadal oscillation focused both in the extratropical North Atlantic (40°–60°N) and also the tropical North Atlantic (0°–20°N). During the warm phase of redefined AMO, most of the United States, especially the eastern United States, is drier than normal (Nigam et al. 2011). Using a climate model and dividing the North Atlantic into the tropical North Atlantic (0°–30°N) and extratropical North Atlantic (30°–70°N), Sutton and Hodson (2005, 2007) concluded that the tropical North Atlantic SSTs are more important to North American precipitation than the extratropical North Atlantic SSTs (Figs. 3, 4 of Sutton and Hodson 2007).

Compared to the large atmospheric internal variability, the impact of SST on the atmosphere can be relatively small and difficult to extract. Based on stochastic climate theory, Frankignoul and Hasselmann (1977) developed a univariate statistical method, equilibrium feedback assessment (EFA), to assess the local impact of SST on the overlying atmosphere (Frankignoul et al. 1998). Later, this method was used to study SST's impact on air–sea fluxes (Frankignoul and Kestenare 2002), atmospheric response to North Pacific SST (Liu and Wu 2004), and vegetation's feedback on global and U.S. climate (Liu et al. 2006; Notaro et al. 2006). The EFA

method was validated using a simple conceptual model by Liu et al. (2006), an ocean–atmosphere general circulation model (Liu and Wu 2004), and a fully coupled atmosphere–ocean–land model (Notaro and Liu 2008; Notaro et al. 2008). Although the EFA method can extract the impact of SST (or vegetation) on the atmosphere, it is a univariate method and cannot distinguish the impact of an individual forcing when there are many factors that concurrently influence the atmosphere. For example, Sun and Wang (2012) studied the impact of soil moisture on precipitation using the EFA method. They concluded that, because of the synchronous oceanic influences on precipitation, EFA cannot separate the influences of soil moisture from that of the oceans, so the impacts of soil moisture on precipitation cannot be estimated using EFA. Liu et al. (2008) further generalized the EFA method, and this multivariate statistical method can distinguish an individual SST mode's impact on the atmosphere. Wen et al. (2010) applied this generalized EFA (GEFA) approach to assess the observed response of 250–850-hPa geopotential height to global SST modes. Zhong et al. (2011) used GEFA to analyze the global ocean's impact on observed U.S. precipitation, focusing for each SST mode on the season when this SST mode has the greatest impacts.

The goal of this paper is to extract the impacts of key SST modes and identify the oceanic modes that most significantly influence North American climate. The perspective is different from Zhong et al. (2011) by focusing on the dominant modes by season, extending the analysis to both surface air temperature and precipitation, and validating the GEFA method using a fully coupled climate model prior to applying it to observations. By focusing on dominant modes by season, this study targets seasonal climate prediction. The paper is arranged as follows: Observational data and the global climate model used in this study are introduced in section 2. In section 3, the statistical method, GEFA, is described and validated. Section 4 identifies the most important SST modes to North American climate. The summary and discussions are presented in section 5.

2. Observations and model

a. Observations and reanalysis

Monthly observed terrestrial surface air temperature and precipitation (Willmott and Matsuura 1995) on a $0.5° \times 0.5°$ grid from 1900 to 2008 are provided by the University of Delaware and used to assess the response of North American climate to observed SST modes. The Hadley Centre Sea Ice and Sea Surface Temperature dataset (HadISST) on a $1° \times 1°$ grid (Rayner et al. 2003) from 1870 to 2011 is applied for identifying oceanic forcing modes. Other monthly variables, such as air temperature, geopotential height, wind, specific humidity, vertical motion, and surface fluxes (include both turbulent and radiation fluxes), are obtained from National Centers for Environmental Prediction–National Center for Atmospheric Research (NCEP–NCAR) Reanalysis 1 (Kalnay et al. 1996) for 1948–2008 to analyze the dynamic mechanisms. The spatial resolution is $2.5° \times 2.5°$, except for the surface fluxes, which are on a T62 Gaussian grid with 192×94 points.

For all observational and reanalysis data, the seasonal cycle and third order polynomial trend are removed to focus on interannual to decadal variability. A 9-point local smoothing method is applied to both surface air temperature and precipitation in order to decrease small-scale noise. Since the sampling error of GEFA decreases with increased sample size (section 3), the length of data that is analyzed in this study is as long as possible. Therefore, when assessing the ocean's influence on surface air temperature and precipitation, a 109-yr time series from 1900 to 2008 is considered; when studying dynamical mechanisms, a 61-yr time series from 1948 to 2008 is used.

b. CCSM3.5

In this study, a fully coupled global climate model is used to validate the statistical GEFA method. The NCAR Community Climate System Model version 3.5 (CCSM3.5) (Collins et al. 2006; Gent et al. 2010) is chosen, which is an interim version of CCSM. The active components applied in this study include the Community Atmosphere Model (CAM3.5), Parallel Ocean Program (POP2), Community Sea Ice Model (CSIM4), and Community Land Model–Dynamic Global Vegetation Model (CLM3.5-DGVM). No flux adjustment is applied. The dynamical core of the atmospheric and land models is the Lin–Rood finite volume dynamical core (Lin 2004), and the horizontal resolution is 2.5° (longitude) $\times$ 1.9° (latitude). The vertical coordinate in CAM is hybrid sigma pressure with 26 layers. CCSM3.5 has been significantly improved compared with previous versions (Gent et al. 2010). For example, the simulated ENSO frequency was improved from a regular 2-yr occurrence in the previous version (Deser et al. 2006) to approximately 3–6-yr intermittent occurrence in version 3.5 (Gent et al. 2010). Also, the global teleconnection pattern forced by ENSO is better represented in the model. Biases in the mean precipitation and double intertropical convergence zone (ITCZ) in the western tropical Pacific Ocean were reduced (Neale et al. 2008).

A multicentury, modern-day simulation (CTL) in equilibrium is produced and the last 100 yr are analyzed. From the CTL run, the statistical GEFA method is used to evaluate the impact of individual oceanic basin's SST modes on North American climate. The model is only applied to validate the GEFA methodology through dynamical experiments, which are described in section 3. As long as the statistical assessment from the CTL run agrees with the dynamical experiments in the same model, it demonstrates that GEFA is reliable and can be applied to observations with some confidence. Therefore, it is unnecessary to compare the simulated and observed results or to validate the simulated climatology.

3. Statistical method and its validation

a. GEFA method

A multivariate statistical method, generalized equilibrium feedback assessment (GEFA), is applied to study the influence of individual SST mode on North American climate. The GEFA method, based on the stochastic climate theory of Frankignoul and Hasselmann (Hasselmann 1976; Frankignoul and Hasselmann 1977), was generalized from univariate to multivariate and formally developed by Liu (Liu et al. 2008; Liu and Wen 2008). The atmospheric response to oceanic forcing based on GEFA has been cross-validated using different statistical methods, such as linear inverse modeling (LIM) and fluctuation–dissipation theorem (FDT) (Liu et al. 2012a,b). Since details of the method have been presented in previous studies (Liu et al. 2008; Wen et al. 2010), they are only briefly summarized here.

The memory of the atmosphere (about 1 week) is shorter than that of SSTs (>1 month). According to Frankignoul et al. (1998), at time scales significantly longer than the atmospheric memory, the response of an atmospheric variable at time t, $\mathbf{A}(t)$ to an oceanic variable $\mathbf{O}(t)$ can be approximated as

$$\mathbf{A}(t) = \mathbf{B} \times \mathbf{O}(t) + \mathbf{N}(t), \tag{1}$$

where N is the atmospheric internal variability and $\mathbf{B}$ is the feedback matrix. If the SST pattern is known, the atmospheric response pattern can be obtained by multiplying the SST pattern with this feedback matrix. Because SST variability at a previous time $\mathbf{O}(t - \tau)$ does not correlate with current atmospheric internal variability $\mathbf{N}(t)$, it is concluded that $\langle \mathbf{O}(t - \tau), \mathbf{N}(t) \rangle = 0$, where $\langle a, b \rangle$ indicates the covariance between variables a and b. Therefore, the feedback matrix $\mathbf{B}$ can be computed by applying covariance to both sides of Eq. (1), resulting in

$$\mathbf{B} = \frac{\langle \mathbf{A}(t), \mathbf{O}(t-\tau) \rangle}{\langle \mathbf{O}(t), \mathbf{O}(t-\tau) \rangle}, \quad \tau > 0, \tag{2}$$

where τ is the time lag, which should be longer than the atmospheric persistence time. From Eq. (1), it is evident that coefficient matrix $\mathbf{B}$ represents the instantaneous atmospheric response to a slowly evolving forcing term (e.g., SST, vegetation).

For a finite sample size, the sampling error increases with lag because of the decreasing autocovariance of $\langle \mathbf{O}(t), \mathbf{O}(t - \tau) \rangle$; therefore, the first lag is preferred, and the pattern of lag 2 is compared with lag 1 to check for consistency. Also, if the forcing fields are highly correlated, then the denominator of $\mathbf{B}$ tends to be singular and a large sampling error can result. An effective way to reduce this kind of sampling error is to perform GEFA in a truncated SST empirical orthogonal function (EOF) space, using only the first several leading EOF modes (Liu and Wen 2008). In this paper, the global ocean is divided into five nonoverlapping ocean basins, following Wen et al. (2010): the tropical Pacific (TP; 20°S–20°N, 120°E–60°W), North Pacific (NP; 20°–60°N, 120°E–60°W), tropical Indian (TI; 20°S–20°N, 35°–120°E), tropical Atlantic (TA; 20°S–20°N, 65°W–15°E), and North Atlantic (NA; 20°–60°N, 100°W–20°E). For most of these ocean basins, the leading two EOF modes have relatively clear physical meanings. The Southern Ocean basins are not considered because in situ data are sparse, and the time series of the dominant modes in South Pacific SSTs are closely correlated with tropical Pacific SSTs, which tend to increase the sampling error in GEFA. The corresponding principal components (PCs) for these five ocean basins are combined into a single forcing matrix,

$$\mathbf{O} = [\text{TP1} \quad \text{TP2} \quad \text{NP1} \quad \text{NP2} \quad \text{TI1} \quad \text{TI2} \quad \text{TA1} \quad \text{TA2} \quad \text{NA1} \quad \text{NA2}], \tag{3}$$

where 1 and 2 indicate the first and second PCs, respectively.

The statistical significance of $\mathbf{B}$ is estimated using the Monte Carlo bootstrap approach (Czaja and Frankignoul 2002). The atmospheric field is scrambled randomly 1000 times by year, and GEFA coefficients are computed using these scrambled atmospheric time series. The significance is determined at each grid cell by the

percentage of GEFA coefficients from the scrambled time series that are smaller in magnitude than the GEFA coefficient from the original time series. Here, 90% is chosen as the significant level.

Seasonal GEFA feedback coefficients are computed as follows. First, monthly GEFA coefficients are computed. For an example, the January GEFA feedback matrix is computed using data from December and January as follows:

$$\mathbf{B}(\text{Jan}) = \frac{\langle \mathbf{A}(\text{Jan}), \mathbf{O}(\text{Dec}) \rangle}{\langle \mathbf{O}(\text{Jan}), \mathbf{O}(\text{Dec}) \rangle}. \quad (4)$$

Then, the wintertime [December–February (DJF)] atmospheric response is calculated as

$$\mathbf{B}(\text{DJF}) = \frac{\mathbf{B}(\text{Dec}) + \mathbf{B}(\text{Jan}) + \mathbf{B}(\text{Feb})}{3}. \quad (5)$$

The other seasons are treated in a similar fashion. Equations (1), (2), (4), and (5) are also suitable for EFA, except the oceanic forcing term $\mathbf{O}(t)$ and feedback coefficient $\mathbf{B}(t)$ are vectors not matrices.

There are several advantages to GEFA over traditional methods. First, GEFA can quantify the impact of each forcing in a unified framework with no need to consider the relationship among the forcings, with no need to have a priori knowledge of the importance of the multiple forcings (Wen et al. 2010). Second, the method is easily applied, with no need for computationally expensive model experiments. Finally, in the real world, there is only one realization of climate, so only a statistical method can be used. In the meantime, there are also some disadvantages to GEFA. First, as for all other statistical methods, GEFA is based on certain assumptions, such as linear relationship between the forcing and response fields. Therefore, the results shown in this paper should be understood as the first-order linear approximation of the feedback response. Second, the accuracy of the method is limited by sampling error, so in this paper τ is set to 1 month and truncated EOFs are applied. As discussed by Wen et al. (2010), Liu et al. (2008), and Liu and Wen (2008), this selection usually gives an optimal assessment.

b. Method validation

The GEFA method will be first validated using the fully coupled climate model, CCSM3.5, in two steps. First, the ability of GEFA to separate the impact of an individual SST mode is demonstrated by examining both the response field and the regression field of the forcing with other forcings. Second, statistical GEFA results from CTL run are compared with results from dynamical experiments.

1) GEFA's ability to separate the response to individual SST mode

The atmosphere is simultaneously affected by multiple SST modes. Since these different SST modes can be correlated, the traditional univariate EFA method cannot separate the impact of each individual SST mode and the GEFA approach is needed. Since there are multiple SST modes concurrently affecting the atmosphere, if we compute a response pattern by regression, it is difficult to associate this response to a specific SST mode. Here, surface temperature (TS) is examined, which is a unique variable since it represents ground temperature over land and SST over ocean. The GEFA coefficient represents the response pattern only when the memory, or temporal autocorrelation, is substantially longer in the forcing (ocean) than the response (atmosphere) variables. Therefore, the EFA or GEFA pattern over land is the response pattern of TS, while over the ocean it is simply the regression of the forcing SST mode to global SSTs. In other words, over the ocean, it indicates the potential relationship between the specific SST mode of interest and global SSTs. Here, as an example, we will examine the first EOF modes of TP (TP1) and TA (TA1) in CCSM3.5 and compare the TS response using EFA and GEFA, respectively. For each specific SST mode, both the EFA and GEFA results are considered for illustration purposes, given that only the latter approach removes the effects of other correlated SST modes.

The first EOF mode of tropical Pacific SST in CCSM3.5 is ENSO (Fig. 1a). During winter (DJF), its impact on TS across North America, based on EFA, includes a warm anomaly over northern North America and a cold anomaly over southern North America (Fig. 1c). Over the ocean, the ENSO pattern over the tropical Pacific, obtained through EFA (Fig. 1c), reproduces the forcing pattern shown in Fig. 1a. Besides the ENSO signal, the Indian Ocean dipole (IOD) mode, the Atlantic Niño mode, and a weak horseshoe pattern in the North Pacific also emerge in the TS pattern. This indicates that the response pattern of TS over land from EFA is actually the result of all of these oceanic forcings, not just TP1. Therefore, EFA cannot isolate the influence of the TP1 mode alone on North American climate.

The first EOF mode of tropical Atlantic SST in CCSM3.5 is the Atlantic Niño mode (Fig. 1b). Its impact on North American TS using EFA method (Fig. 1d) is very similar with that of ENSO (Fig. 1c). Over the ocean, EFA detects the Atlantic Niño mode but also the ENSO mode, IOD mode, and the North Pacific horseshoe pattern. This indicates that the response pattern over land from EFA (Fig. 1d) incorporates all of these

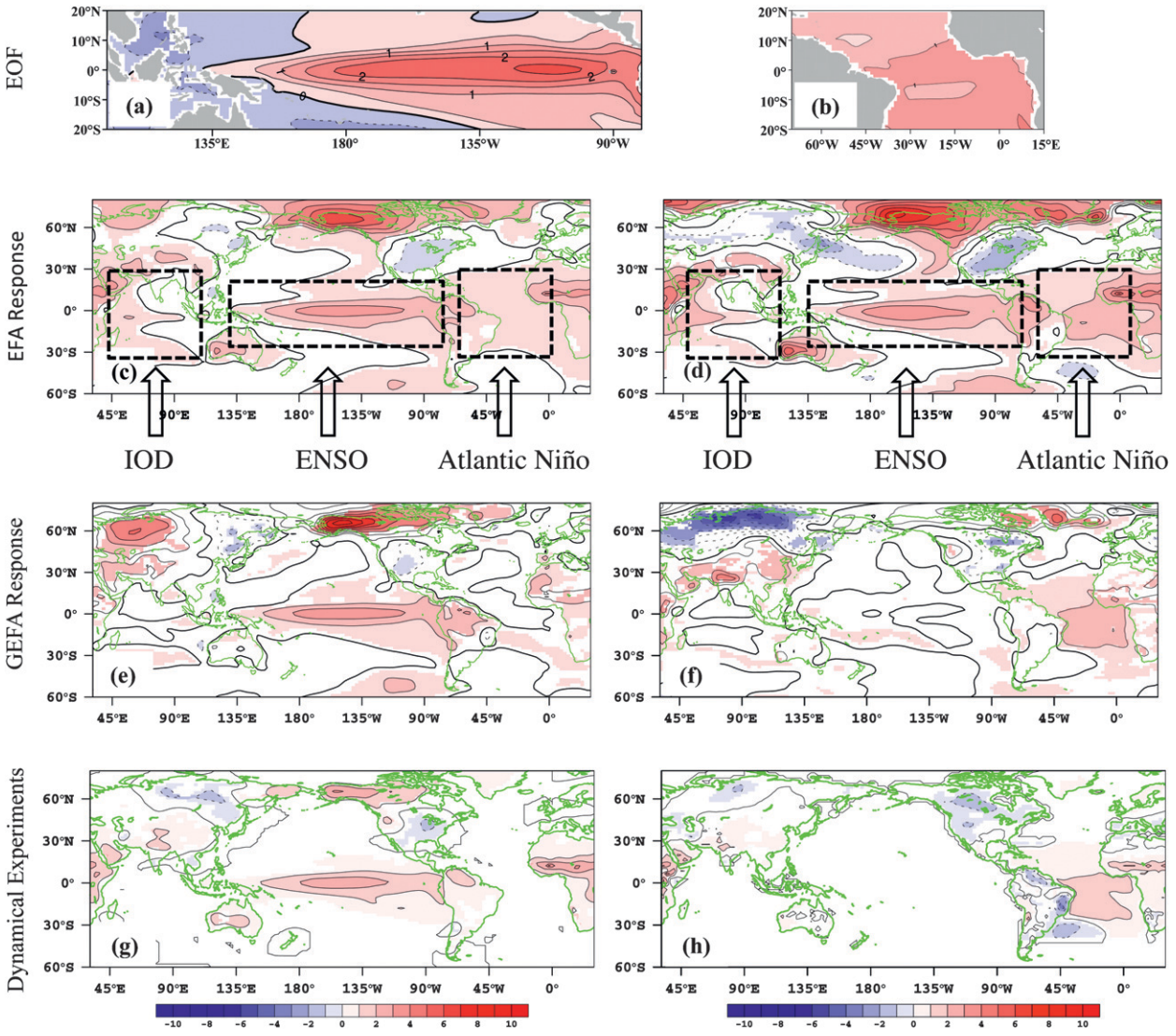

FIG. 1. Spatial pattern of the first EOF mode of (a) tropical Pacific (TP1) and (b) tropical Atlantic (TA1) SSTs in the model. Wintertime (DJF) TS response to (left) TP1 and (right) TA1 using (c),(d) EFA; (e),(f) GEFA; and (g),(h) dynamical experiments. Shading in (c)–(f) indicates ≥90% significance based on Monte Carlo test. Shading in (g),(h) indicates ≥90% significance based on a *t* test. The panels (a),(b) are unitless, and units of (c),(d) are °C °C^{-1}. Black boxes in (c),(d) indicate IOB, ENSO, and Atlantic Niño modes.

oceanic forcings, not just the Atlantic Niño. As a result, the impacts of TP1 and TA1 on global TS based on EFA are unrealistically similar, and EFA fails to isolate the impact of Atlantic Niño.

For further exploration, we expand the forcing field to include the leading two PCs in each ocean basin, as in Eq. (3), and apply GEFA. The GEFA response pattern of TS to ENSO forcing (Fig. 1e) is still similar with the EFA results (Fig. 1c), but over the ocean the ENSO mode remains while the IOD mode, Atlantic Niño mode, and North Pacific horseshoe pattern disappear. With GEFA, all other oceanic signals except ENSO are very weak. The GEFA pattern of TS to TA1 forcing (Fig. 1f) is significantly different from that of EFA (Fig. 1d). Over North America, GEFA identifies a cold anomaly over northern North America. Over the oceans, except for the Atlantic Niño mode, all other oceanic modes are absent. In other words, GEFA (Figs. 1e,f) can successfully extract an individual SST mode's impact on the atmosphere. The similarity between the TS response to ENSO forcing using EFA and GEFA indicates that the ENSO signal dominants over other SST modes, so when using EFA, although the impacts of other SST modes still exist, they are overwhelmed by ENSO. The significant difference between the TS response to Atlantic Niño mode using EFA and GEFA demonstrates that GEFA can extract the influences of the tropical Atlantic SST mode on the atmosphere, while EFA cannot. Although we have

TABLE 1. Spatial correlation of the global response pattern of geopotential height, surface air temperature, and precipitation to the ENSO forcing between dynamical and statistical assessment by season [DFJ, MAM, JJA, and September–November (SON)]. When doing correlation both land and ocean values are considered for geopotential height, and only land values are considered for surface air temperature and precipitation.

ENSO	Geopotential height	Surface air temperature	Precipitation
DJF	0.84	0.50	0.67
MAM	0.90	0.70	0.63
JJA	0.90	0.74	0.76
SON	0.64	0.42	0.48

demonstrated that GEFA can separate each individual SST mode's impact in the CTL run, the approach to validation was not as direct as dynamical experiments. Therefore, in the next section, dynamical experiments are described and the statistical and dynamical results are compared.

2) DYNAMICAL ASSESSMENT

The response of the atmosphere to a specified SST forcing can also be obtained in a climate model through ensemble sensitivity experiments, in which an SST anomaly is prescribed. Through ensemble experiments, the atmospheric internal noise is minimized in comparison to the feedback signal. The dynamical experiments are completely independent of the statistical method, thereby providing an independent check of the statistical method. In this study, ENSO and Atlantic Niño modes are chosen for dynamical experiments, since both are believed to significantly influence the climate of the adjoining continental regions (Deser et al. 2006), including North America, based on a prior application of GEFA to CTL.

The 1-yr ensemble experiments are designed, with each ensemble member starting from a different January restart file from the CTL run, and the atmosphere is forced by a prescribed SST and sea ice field. To compare with the statistical results, these prescribed fields should match those in the statistical assessment. Therefore, the monthly GEFA result of TS (Fig. 1e) over the tropical Pacific (20°S–20°N, 120°E–70°W) is superimposed onto a global climatology of SSTs from CTL. The prescribed sea ice field is the climatological sea ice fraction from CTL. A comparison of the SST pattern in Figs. 1e and 1g over the tropical Pacific shows that the pattern and strength of SST anomalies are comparable between GEFA and the dynamic experiments, so both reproduce the ENSO pattern in Fig. 1a. Since the GEFA results reflect the linear portion of the atmospheric response to the SST forcing, when designing the dynamical experiments, both positive (P) and negative (N) phases of the GEFA pattern, each of 25 cases, are superimposed onto the model's global SST climatology. The linear portion of the dynamical response, $(P - N)/2$, is then compared with the model's statistical GEFA results. The Atlantic Niño experiments are designed exactly the same way as the ENSO experiments, except with a different prescribed SST pattern.

TABLE 2. As in Table 1, but for the Atlantic Niño mode.

Atlantic Niño mode	Geopotential height	Surface air temperature	Precipitation
DJF	0.46	0.48	0.70
MAM	0.41	0.26	0.68
JJA	0.58	0.29	0.54
SON	0.63	0.34	0.56

The response of TS over land to ENSO from both statistical and dynamical assessments is very similar (Figs. 1e,g). Both indicate warm anomalies over Africa (peaking over the Sahel), western and southern Eurasia, and Alaska–northern Canada and cool anomalies over northeastern Russia and the central United States associated with the warm phase of ENSO. The spatial correlation between the GEFA (Fig. 1e) and dynamical assessments (Fig. 1g) is 0.50 over the global land. The response of TS over land to TA1 from both statistical (Fig. 1f) and dynamical assessments (Fig. 1h) is also quite consistent, with a spatial correlation of 0.48 over the global land. Both indicate warm anomalies over tropical Africa and southern Eurasia and cool anomalies over northern Europe (not significant in dynamical experiment) and Canada. The spatial correlations of the global response pattern of geopotential height, surface temperature, and precipitation between the dynamical experiments and the statistical assessment to ENSO and TA1 are shown by season in Tables 1 and 2, respectively. The range of spatial correlation is 0.42–0.90 for the ENSO case and 0.26–0.70 for the Atlantic Niño case. All of these correlations can pass the 90% significant level of a t test.

Generally, the statistical and dynamical assessments agree with each other. In the meantime, there are still some inconsistencies. For example, the amplitude of the atmospheric response in the statistical assessment is generally larger than that of the dynamical assessment, especially over high latitudes. There are several possible reasons. First, every statistical assessment, including GEFA, contains sampling error. When SST modes are well correlated, the denominator of $\mathbf{B}$ in Eq. (2) becomes singular and unreliable with an inflated magnitude. Second, the dynamical assessment also has limitations. Since we could not produce unlimited experiments, the atmospheric internal noise was not totally cancelled. Third,

TABLE 3. The three most important observed SST modes for surface air temperature across North America in each season. The number in parentheses (%) reflects the relative importance of this mode among the 10 SST modes. The rightmost column is the sum (%) of the proportion of three SST modes.

Season	Top three important SST modes to surface air temperature			Sum
DJF	TP1 (23)	TI1 (39)	NP1 (17)	79
MAM	TP1 (12)	NA1 (17)	NP1 (20)	49
JJA	TP1 (9)	TI1 (34)	NA1 (18)	61
SON	TA1 (16)	NA2 (34)	NP1 (20)	70

TABLE 4. As in Table 3, but for North American precipitation.

Season	Top three important SST modes to precipitation			Sum
DJF	TP1 (21)	TI1 (23)	TA1 (16)	60
MAM	NP2 (13)	TI1 (18)	TA2 (17)	48
JJA	TP1 (17)	TI1 (12)	TA2 (11)	40
SON	NP1 (16)	TI1 (15)	TA2 (16)	47

since the prescribed sea ice field is set to climatology, the positive feedback between sea ice and surface air temperature is blocked in the dynamical experiments. Fourth, the atmosphere is forced not only by SSTs but also by land–atmosphere interactions related to vegetation, soil moisture, and snow. Fifth, the GEFA results are based on a 100-yr CTL run, which means the response pattern is the 100-yr mean atmospheric response. However, the ensemble experiments are only conducted in first 25 yr because of computational expenses. All of these may contribute to the inconsistencies between the statistical and dynamical assessments.

4. Observational assessment

In section 3, the GEFA method was validated against dynamical experiments and the two methods were shown to be consistent. Now, it will be applied to observational data. The most important SST modes to North American climate are identified and their dynamical mechanisms are explored.

a. Identifying key SST modes

Of the 10 SST modes, 4 are distinctly important to North American climate (Tables 3, 4). TP1 (ENSO mode) and TI1 (Indian Ocean Basin mode) are important for both surface air temperature and precipitation, NP1 is mainly important for temperature, and TA2 is important for precipitation.

The importance of individual SST modes is evaluated as follows: First, the seasonal response of surface air temperature across North America to individual SST forcings is assessed using the GEFA method and significance is evaluated with Monte Carlo tests. For each season, each SST mode corresponds to a determined response pattern. Second, the number of significant grid cells is counted, with the percentage of significant cells to the total grid cells over North America representing the range of influence of a specific SST mode. Third, the absolute values of GEFA coefficients for significant grid cells are added together, then multiplied by the standard deviation of the corresponding principal component; this represents the response strength to a specific SST mode. Finally, considering both the range of influence and strength of impact, the three most important SST modes to observed surface air temperature, by season, are shown in Table 3. In general, the same critical SST modes are identified whether the basis is on range of influence or strength of impact. The same procedure is applied to precipitation, as shown in Table 4. In each season, the relative importance of each SST mode is the percentage of one specific SST mode's impact to the total SST modes' impact. The three leading modes represent roughly 50% of the total influence of global oceans on North American climate. The importance of SST modes is evaluated at other spatial resolutions (e.g., atmospheric data on 2.5° × 2.5°), and the results are consistent. Now, we will individually discuss the important SST modes, focusing on the seasons with their largest impact.

b. ENSO mode

ENSO is the first EOF mode of the tropical Pacific SSTs (Fig. 2a), explaining 54% of monthly anomaly variance. The standard deviation of the corresponding PC is 0.37°C. The GEFA coefficient in Eq. (2) has units of °C (std dev of PC)$^{-1}$, so by multiplying this coefficient by the standard deviation of the corresponding PC the actual magnitude of the impact is quantified. The influence of ENSO on North American climate is strongest during winter and weakest during autumn. Here, winter and summer are examined.

1) TP1: WINTER (DJF)

During winter, the surface air temperature pattern associated with the warm phase of ENSO (Fig. 2a) is characterized by anomalous warm air over northern United States and Canada and anomalous cold air over the southern United States and Mexico (Fig. 3a). The warm anomaly peaks over British Columbia, Alberta, and the U.S. Pacific Northwest, with a maximum value of 3.53°C °C^{-1} × 0.37°C = 1.31°C (where the standard deviation of the corresponding PC is 0.37°C). The cold anomaly peaks over Alabama, Georgia, and Mexico, reaching −2.90°C °C^{-1} × 0.37°C = −1.07°C.

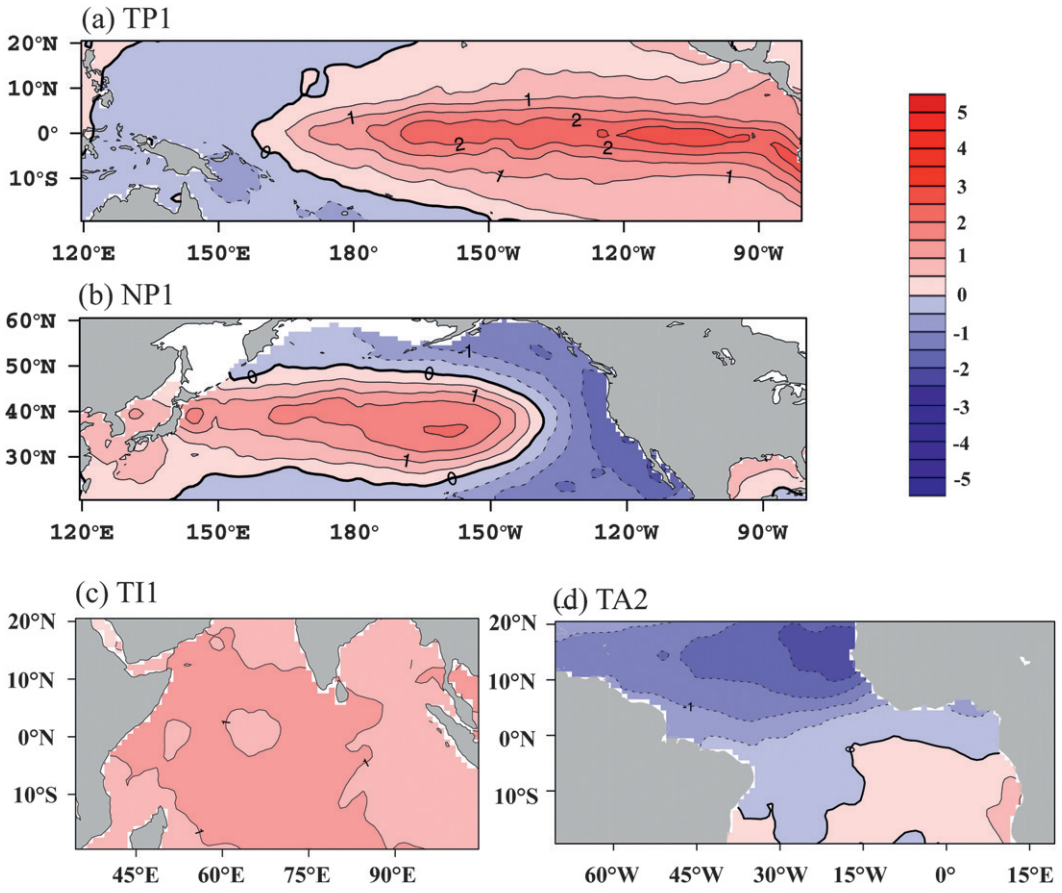

FIG. 2. Observed EOF1 of monthly (a) tropical Pacific, (b) North Pacific, and (c) tropical Indian SST and EOF2 of (d) tropical Atlantic SST (unitless).

These thermal responses can be attributed both to anomalies in temperature advection and downward longwave radiation. During the warm phase of ENSO, a positive Pacific North American (PNA)–like pattern is generated in the mid–high latitudes (Fig. 3c). According to the climatological air temperature (Fig. 3d, shading) and response wind pattern to ENSO (Fig. 3d, vector) at 850 hPa, the anomalously warm air in the U.S. Pacific Northwest is caused by additional heat transport from the maritime Pacific Ocean (Fig. 3d, arrow A). The anomalous warm advection from the North Atlantic (Fig. 3d, arrow C) increases the air temperature in Quebec. The colder air in the southern United States is attributed to anomalous cold advection from the U.S. Northeast (Fig. 3d, arrow D). Besides temperature advection, changes in downward longwave radiation, related to total column water vapor (Fig. 3e) and cloud cover, also contribute to the temperature changes, which is similar with Zhang et al. (2011). The response patterns of surface air temperature (Fig. 3a) and vertically integrated specific humidity (Fig. 3e) are spatially consistent. During winter, the atmospheric water vapor content is largely regulated by air temperature and, through the greenhouse effect of water vapor, more moisture leads to greater downward longwave radiation, which further warms the surface air. For surface air temperature, the most important determining factors are temperature advection and downward longwave radiation, but other factors, such as latent heat flux and downward shortwave radiation, also modify the temperature pattern. For example, over the northern Great Plains, water vapor increases significantly, but surface air temperature does not increase. This may be attributed to the increase in latent heat flux, which causes a decrease in surface air temperature and increase in atmospheric humidity; the decrease in downward shortwave radiation also reduces the air temperature.

During winter, the precipitation pattern associated with the warm phase of ENSO consists of an increase in precipitation in the U.S. Great Plains and the Gulf States and a decrease in Alaska, the western United States, and the Great Lakes Basin (Fig. 3b). The positive precipitation anomaly is largest over the U.S. Southeast, reaching 2.02 mm day^{-1} °C^{-1} × 0.37°C = 0.75 mm day^{-1}. The

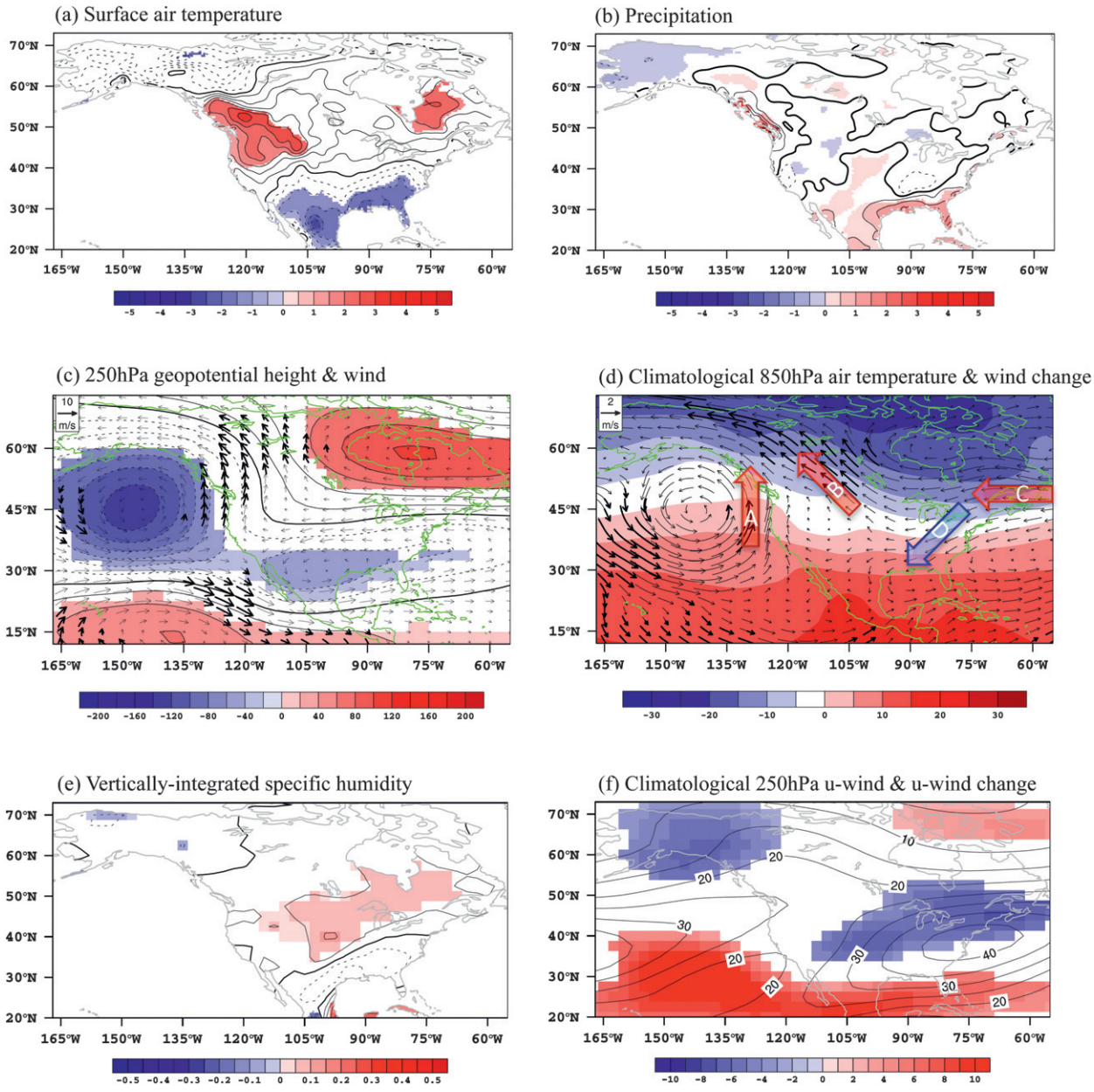

FIG. 3. The response of (a) surface air temperature (°C °C^{-1}), (b) precipitation (mm day^{-1} °C^{-1}), (c) 250-hPa geopotential height (m °C^{-1}) and wind (m s^{-1} °C^{-1}), (d) 850-hPa wind (vector; m s^{-1} °C^{-1}) and climatological winter air temperature (shading; °C), (e) vertically integrated specific humidity (kg kg^{-1} °C^{-1}), and (f) 250-hPa u wind (shading; m s^{-1} °C^{-1}) and climatological u wind (contours; m s^{-1}) to warm phase of ENSO (Fig. 2a) during winter in the observations. Shading [except in (d)] and thick black vector arrows indicate ≥90% statistical significance based on Monte Carlo tests. The thick arrows A, B, C, and D in (d) represent temperature advection, with blue for cold advection and red for warm advection.

precipitation deficit is greatest over California and Nevada, reaching -1.36 mm day^{-1} °C^{-1} × 0.37°C = -0.50 mm day^{-1}. The increase in precipitation over Mexico and the U.S. Southeast is related to a southward shift of the subtropical jet (Fig. 3f), which supports more synoptic storms and precipitation (Neelin 2011). In addition, the southward-shifted subtropical jet stream enhances the westerly wind within 20°–30°N and its associated secondary ageostrophic circulation. This anomalous circulation includes ageostrophic northerly wind with ascending air in the right entrance region and descending air in the left entrance region. This secondary circulation induces more precipitation in equatorward side of the jet entrance region and less precipitation in the polar side of the jet entrance region, corresponding to drier conditions over the Great Lake Basin (Eichler and

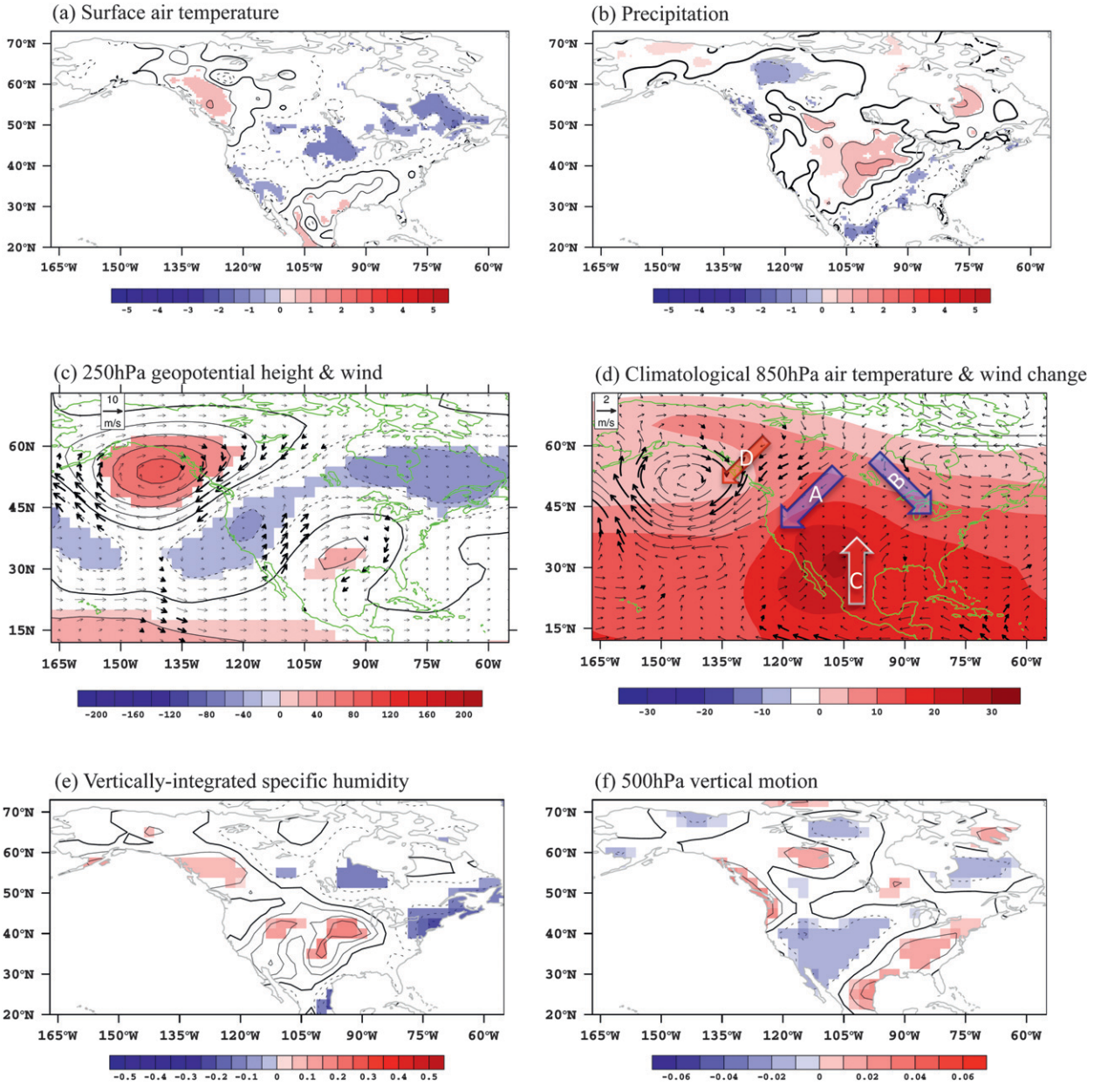

FIG. 4. As in Fig. 3, but for the warm phase of ENSO (Fig. 2a) during summer in the observations; and (d) the 850-hPa climatological summer air temperature and (f) 500-hPa vertical motion (Pa s^{-1} $°C^{-1}$; negative means ascending).

Higgins 2006; Holton 1979; Webster and Fasullo 2003). The increase in precipitation over western Canada is mainly caused by anomalous ascending motion (not shown). Although the column atmospheric moisture hardly changes, the climatological moisture is abundant there; therefore, the anomalous ascent supports more precipitation.

2) TP1: SUMMER (JJA)

During the warm phase of ENSO, summertime [June–August (JJA)] precipitation increases particularly over the U.S. Great Plains and decreases over the eastern United States (Fig. 4b). The precipitation departures range from 1.59 mm day^{-1} $°C^{-1}$ × 0.37°C = 0.59 mm day^{-1} to −3.38 mm day^{-1} $°C^{-1}$ × 0.37°C = −1.25 mm day^{-1}. The precipitation response is caused by changes in both atmospheric vertical motion and moisture advection. The summertime response pattern of geopotential height to the warm phase of ENSO (Fig. 4c) is quite different from that of winter. It consists of a positive height anomaly over the Aleutian low region, a negative anomaly extending from the U.S. Southwest to Quebec,

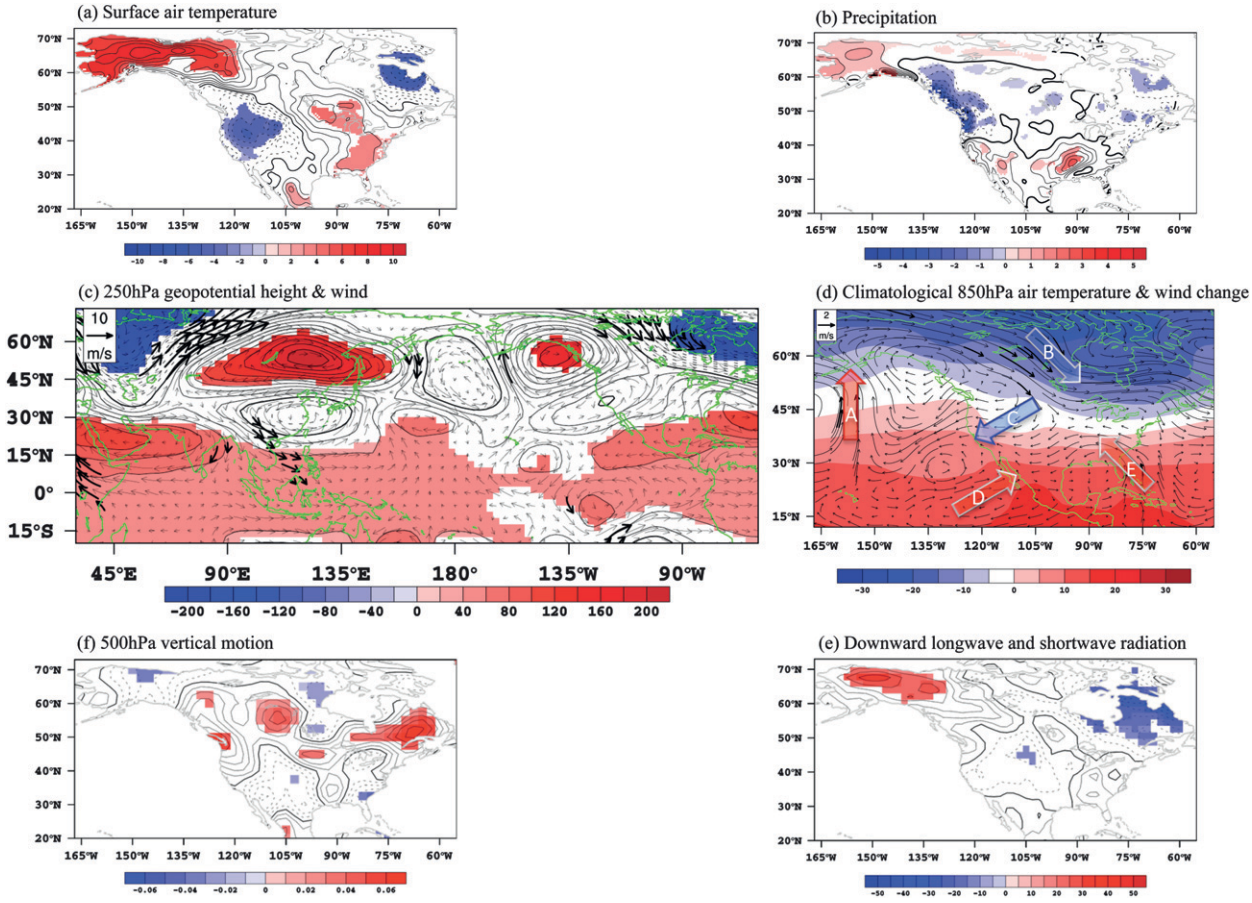

FIG. 5. As in Fig. 4, but the response to warm phase of IOB (Fig. 2c) during winter; and (e) the response of downward longwave and shortwave radiation (W m^{-2} $°C^{-1}$).

and a weak positive anomaly over the southern United States. This anomalous atmospheric circulation determines the pattern of vertical motion, with high (low) pressure corresponding to descent (ascent). Summertime precipitation in the Great Plains is enhanced because of a strengthened low-level jet (Fig. 4d, arrow C), which brings moisture from the Gulf of Mexico to the region (Fig. 4e), and anomalous ascent (Fig. 4f), while the decrease in precipitation in the eastern United States is mainly caused by anomalous descent.

During summer, the surface air temperature pattern associated with the warm phase of ENSO includes a large area of anomalous cold air extending from the U.S. Southwest to eastern Canada (Fig. 4a). The cooling peaks at $-1.54°C\ °C^{-1} \times 0.37°C = -0.57°C$ over the U.S. Great Plains. The response pattern of surface air temperature follows that of precipitation (Figs. 4a,b), with positive precipitation anomalies associated with negative temperature anomalies. The temperature pattern is determined largely by downward shortwave radiation (not shown; similar to precipitation but with the opposite sign), which is related to cloud cover (not shown; similar to precipitation), and temperature advection (Fig. 4d, arrows A and B).

Qualitatively, our results are consistent with previous studies regarding the impact of ENSO on North American climate. The surface air temperature and precipitation patterns during winter agree with studies by Ropelewski and Halpert (1986, 1987), Halpert and Ropelewski (1992), Kiladis and Diaz (1989), and Zhang et al. (2011). The precipitation pattern during summer is consistent with studies by Ting and Wang (1997), Barlow et al. (2001), and Hoerling and Kumar (2003). In this study, we further quantified these impacts over North America. The influence of ENSO on the atmosphere is relatively easy to extract, since its variability is strong and it dominates the interannual variability in the coupled atmosphere ocean system.

c. *Tropical IOB mode*

The first EOF mode of tropical Indian SSTs is the Indian Ocean Basin mode or Indian Ocean monopole

mode (Fig. 2c). It explains 41% of the monthly anomaly variance, and the standard deviation of its corresponding PC is 0.20°C. The IOB mode significantly affects winter and summer air temperature and year-round precipitation across large areas of North America. Surprisingly, its impact on surface air temperature across North America even exceeds that of ENSO during both winter and summer (Table 3).

1) TI1: WINTER (DJF)

During winter, the positive IOB mode (Fig. 2c) results in warm air anomalies over Alaska, northwest Canada, the Great Lakes Basin, the U.S. Southeast, and Mexico and cold air anomalies over the western United States and northern Quebec (Fig. 5a). The warm air anomalies peak over Alaska at about $12.46°C\ °C^{-1} \times 0.20°C = 2.49°C$. The cold air anomalies are greatest over northern Quebec, reaching $-8.22°C\ °C^{-1} \times 0.20°C = -1.64°C$. The surface air temperature response to the IOB mode can be attributed to anomalies in temperature advection and downward longwave and shortwave radiation. During the positive phase of IOB, over the Indian Ocean, the atmospheric local response is baroclinic, with a low pressure anomaly at a low level (850 hPa; not shown) and a high pressure anomaly at a high level (250 hPa; Fig. 5c). The local atmospheric response can be explained by the Gill model (Gill 1980). At midlatitude, the response pattern of atmosphere is equivalent barotropic wave trains. The mechanism of these wave trains is related to the atmospheric eddy–mean flow interactions (Peng et al. 1995; Peng and Whitaker 1999). Over North America the response pattern of 250-hPa geopotential heights consists of a low–high–low over the northwest Pacific, northeast Pacific and Gulf of Alaska, and Hudson Bay (Fig. 5c). The corresponding southerly wind anomaly (Fig. 5d, arrow A) transfers anomalously warm, moist air from the Pacific Ocean to Alaska. A northeasterly wind anomaly (Fig. 5d, arrow B) brings colder, drier air from the polar regions to Quebec. The positive height anomaly at 850 hPa over the Gulf of Alaska extends to the central United States, producing cold, dry advection (Fig. 5d, arrow C) into the western United States. In the subtropics, negative height anomalies are generated near the Gulf of California, which transport warmer, wetter air into Mexico (Fig. 5d, arrow D), and near the Gulf of Mexico, which support positive anomalies of temperature and moisture advection (Fig. 5d, arrow E) into the U.S. Southeast. The temperature pattern is also regulated by downward longwave and shortwave radiation (Fig. 5e).

Wintertime precipitation anomalies associated with the positive phase of the IOB mode include drier conditions across Canada and the northern United States and wetter conditions across Alaska and the southern United States (Fig. 5b). The most severe drying occurs near British Columbia, Washington, and Oregon, with a maximum precipitation deficit of $-7.58\ \text{mm day}^{-1}\ °C^{-1} \times 0.20°C = -1.52\ \text{mm day}^{-1}$. The wettest anomalies occur over Arkansas, with a maximum surplus of $4.53\ \text{mm day}^{-1}\ °C^{-1} \times 0.20°C = 0.91\ \text{mm day}^{-1}$. The precipitation deficit over British Columbia and Quebec is caused by a negative anomaly in moisture advection (northerly wind from polar regions) and subsidence associated with an anomalous high. The precipitation surplus over Arkansas is mainly caused by enhanced moisture advection from the Atlantic Ocean (Fig. 5d, arrow E).

2) TI1: SUMMER (JJA)

During summer, the response of surface air temperature to the positive phase of IOB mode (Fig. 2c) includes broad warming north of 40°N and cooling over Texas and Mexico (Fig. 6a). The warming is mostly uniform in strength between 40° and 60°N, reaching $4.08°C\ °C^{-1} \times 0.20°C = 0.82°C$, and amplitude of cooling is about $-4.09°C\ °C^{-1} \times 0.20°C = -0.82°C$ around Texas. Summertime precipitation is reduced over the U.S. Great Plains and Quebec. The most severe drought conditions are found over Nebraska, Iowa, Missouri, and Kansas, with precipitation deficits reaching $-4.42\ \text{mm day}^{-1}\ °C^{-1} \times 0.20°C = -0.88\ \text{mm day}^{-1}$. Precipitation increases along the Gulf of Mexico, with surpluses that reach $4.51\ \text{mm day}^{-1}\ °C^{-1} \times 0.20°C = 0.90\ \text{mm day}^{-1}$ (Fig. 6b).

The surface air temperature and precipitation patterns are related to the anomalous large-scale geopotential height. During summer, when Indian Ocean SSTs are greater than normal, a circumglobal wave train is generated across the North Hemispheric midlatitudes (Yang et al. 2009; Ding et al. 2011), which includes an anomalous high over the North American midlatitudes (Fig. 6c). The corresponding temperature advection (Fig. 6d, arrow B) and downward longwave radiation (not shown; similar to Fig. 6e) are responsible for this temperature response pattern. The descending motion associated with the anomalous high over the Great Plains hinders precipitation, while the northerly wind anomaly (Fig. 6d, arrows C and D) weakens the low-level jet, limiting moisture transport from the Gulf of Mexico. Both conditions favor summertime drought over the Great Plains.

The results for the IOB mode confirm that the Indian Ocean indeed has a strong impact on North American climate. A combination of the warm phase of IOB mode and cold phase of ENSO can cause large-scale drought across North America in either winter or summer, which is consistent with the study by Hoerling and Kumar (2003). Compared with ENSO's impact on surface air temperature, IOB has a greater impact across North

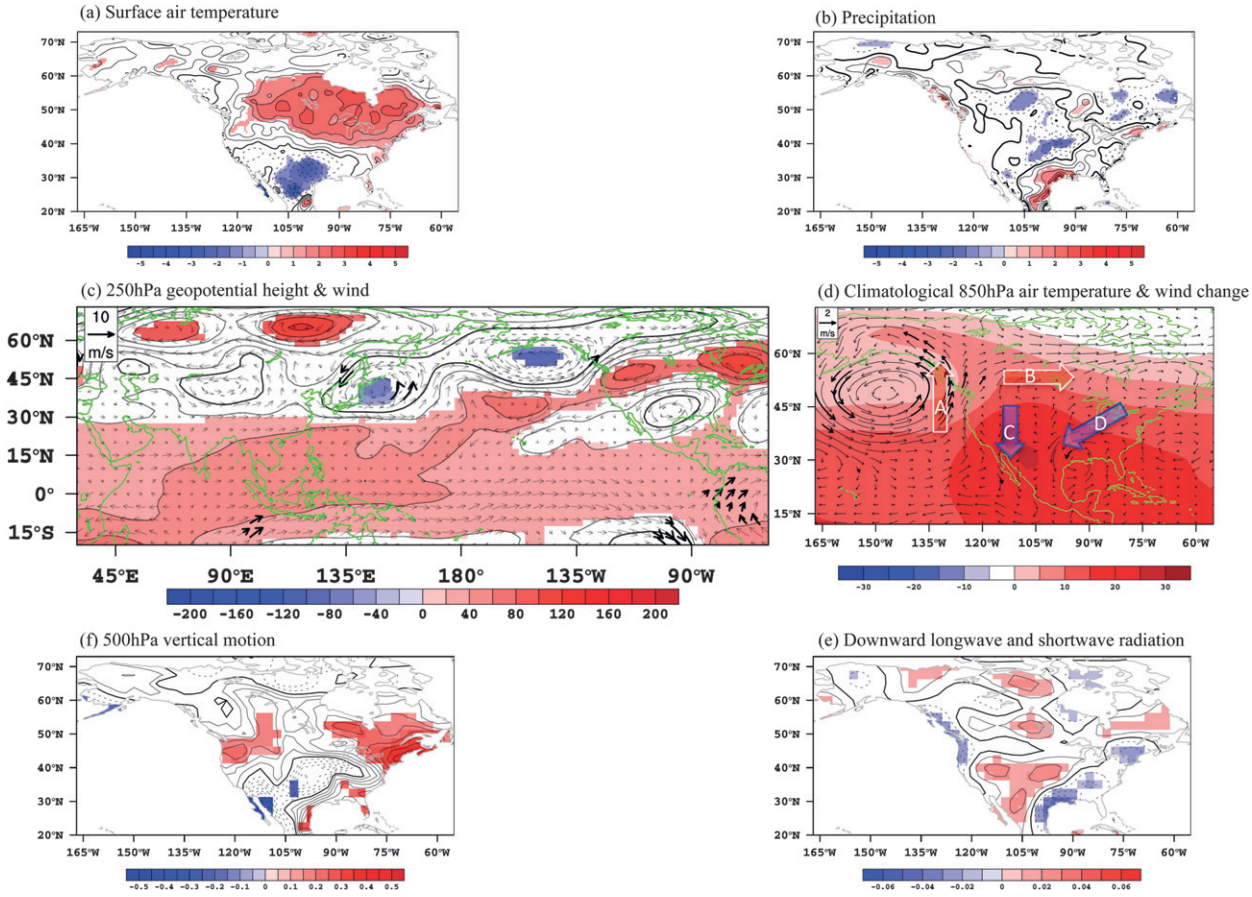

FIG. 6. As in Fig. 4, but the response to warm phase of IOB during summer.

America during both winter and summer. This is has not been demonstrated by previous studies, likely since the IOB mode is correlated with ENSO (Yang et al. 2007), and previous studies could not separate its impact from that of ENSO clearly.

d. North Pacific first EOF mode

The leading mode of North Pacific SST is a basinwide horseshoes pattern with warm anomalies in the Kuroshio–Oyashio Extension (KOE) region and cold anomalies surrounding this zone (Fig. 2b). It can explain 26% of the year-round SST variance, and the standard deviation of its corresponding PC is 0.27°C. NP1 mainly affects surface air temperature in North America from autumn to spring. Here, the discussion focuses on winter and spring.

During winter, the response pattern of surface air temperature to NP1 forcing (Fig. 2b) consists of cold anomalies over western North America and northern Quebec and warm anomalies over the U.S. Northeast (Fig. 7a). The cold anomaly peaks over Alaska and the Yukon at $-4.88°C\ °C^{-1} \times 0.27°C = -1.32°C$, while the warm anomaly in the U.S. Northeast reaches $3.04°C\ °C^{-1} \times 0.27°C = 0.82°C$. The response pattern of surface air temperature to NP1 forcing is mainly determined by anomalous temperature advection. A positive KOE SST anomaly locally forces a ridge (Liu and Wu 2004), which further stimulates a positive North Atlantic Oscillation (NAO) downstream (below-normal heights across the high latitudes and above-normal heights over the central North Atlantic) through the Aleutian low–Icelandic low seesaw (Honda et al. 2005) (Fig. 7c). The combination of a weaker Aleutian low and stronger Icelandic low favors cold advection into much of North America, particularly its western regions (Figs. 7a,c). The strengthened Bermuda high, under positive NAO, creates mild conditions in the eastern United States (Figs. 7a,c). During spring, the anomalous area of cooling spreads eastward (Fig. 7b), peaking at $-3.86°C\ °C^{-1} \times 0.27°C = -1.04°C$ over Alberta and Saskatchewan (Fig. 7b). The anomalous high response to the NP1 forcing spreads eastward, such that the cold air from polar regions can easily advance southward, leading to cold conditions across North America.

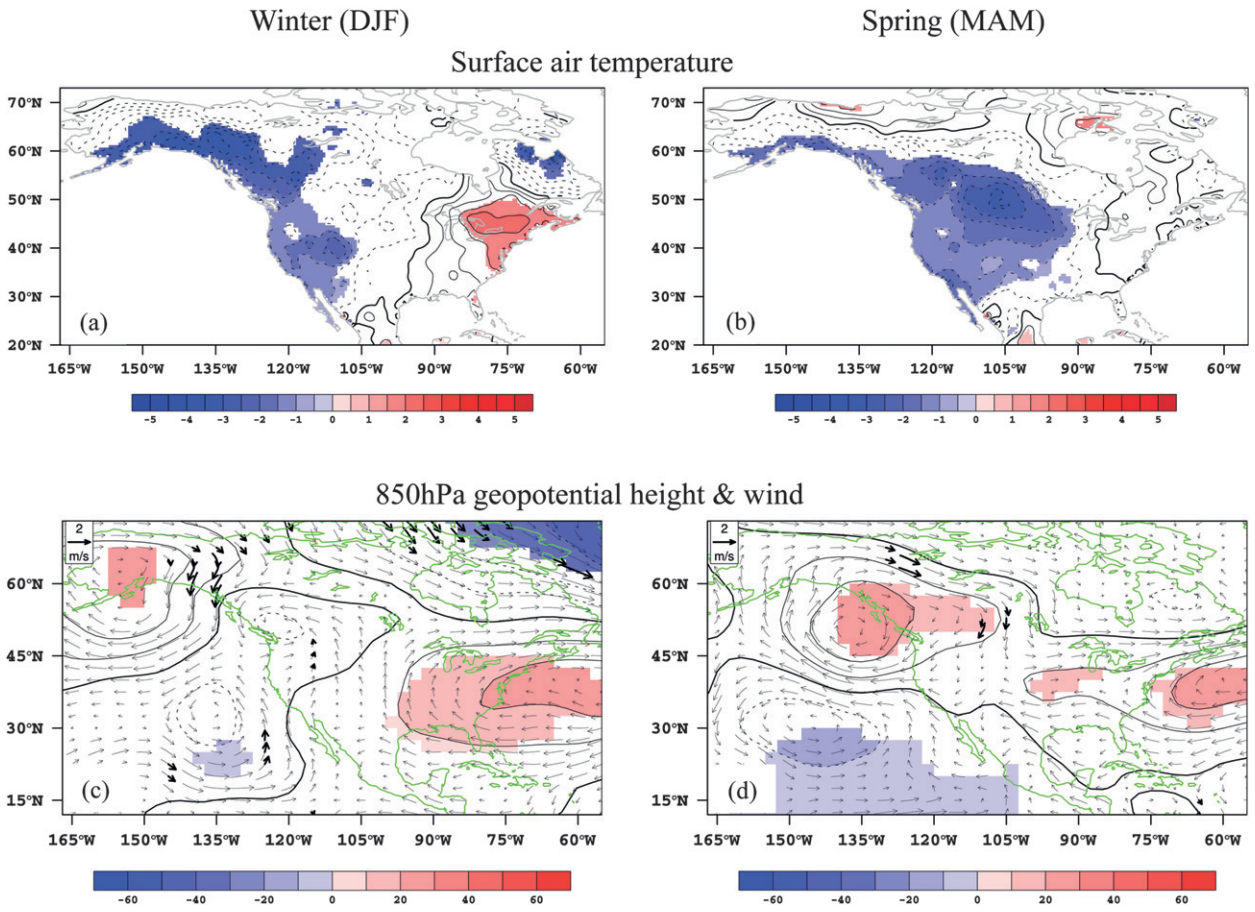

FIG. 7. The response of (top) surface air temperature (°C °C^{-1}) and (bottom) 850-hPa geopotential height and wind (m °C^{-1}) to the NP1 forcing (Fig. 2b) during (left) winter and (right) spring. Shading and thick black arrows indicate ≥90% statistical significance based on Monte Carlo tests.

The observed influences of NP1 on wintertime surface air temperature and precipitation, as determined by GEFA, are somehow different from previous studies by Mantua et al. (1997) and Mantua and Hare (2002). Using composite analysis, Mantua et al. (1997, their Fig. 3a) found that, if the KOE SSTs are lower than normal, then the surface air temperature is anomalously high over northwestern North America and anomalously low over the U.S. Southeast and Mexico. They also found that the atmosphere is drier over the zonal band of 40°–60°N and wetter over the U.S. Southwest and Mexico (their Fig. 3b). The strong warming over Alaska resembles our GEFA-based response to IOB forcing (Fig. 5a), and the cooling over the U.S. Southeast and Mexico resembles our GEFA-based response to ENSO forcing (Fig. 3a). Therefore, the linear combination of the responses to the warm phase of ENSO, warm phase of IOB, and cold phase of NP1 is computed. This total impacts of ENSO, IOB, and NP1 on surface air temperature (Fig. 8a) and precipitation (Fig. 8b) can reproduce Mantua's results, which indicates that the response that they attributed to PDO might in reality be the result of interactions among ENSO, PDO, and IOB. The advantage of GEFA here is that it can separate the influence of each individual oceanic mode.

e. *Tropical Atlantic second EOF mode*

The second EOF mode of tropical Atlantic SST is characterized by predominant cooling in the tropical North Atlantic (TNA) and weak warming in the southern Atlantic (Fig. 2d) and is sometimes referred to as the tropical Atlantic dipole mode. It can explain 26% of the year-round SST variance, and the standard deviation of its corresponding PC is 0.20°C. TA2 mainly influences North American precipitation from spring to autumn, particularly autumn. During autumn, anomalously low TNA SSTs correspond to wetter conditions across much of the United States, particularly in the east, and drier conditions across Ontario (Fig. 9a). The largest precipitation surplus reaches 5.93 mm day^{-1} °C^{-1} × 0.20°C = 1.19 mm day^{-1}

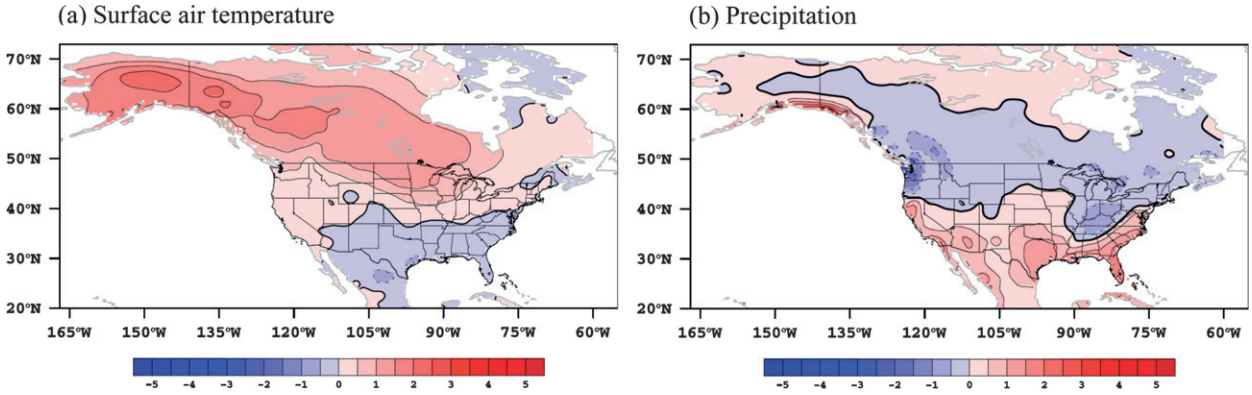

FIG. 8. The wintertime response of (a) surface air temperature (°C) and (b) precipitation (mm day^{-1}) to a combination of TP1, TI1, and negative NP1 weighted by their standard deviation of PC.

in Missouri, Arkansas, and Illinois, while the deficit peaks over Ontario at -2.25 mm day^{-1} °C^{-1} $\times$ 0.2°C = -0.45 mm day^{-1}.

When the TNA SST is anomalous low, the atmosphere responds with baroclinic Rossby waves at the low latitudes (Gill 1980) and equivalent barotropic waves at the mid–high latitudes (Hoskins and Karoly 1981) (Fig. 9c; 250-hPa results not shown). An anomalous trough over central/western North America and ridge over the Caribbean generate strong southerlies from the Gulf of Mexico into the U.S. Southeast, leading to enhanced moisture flux (Fig. 9c). The enhanced moisture flux and anomalous ascending air motion over the eastern United States induce an increase in precipitation. The enhanced southerlies extend to Hudson Bay (Fig. 9c), yet it is anomalously dry there (Fig. 9a). There are two possible reasons. One is due to a secondary circulation induced by a strengthened upper-level westerly jet stream (Fig. 9d). This secondary circulation favors descending motion in the jet's left entrance region and ascending motion in the right entrance region, although the descending air motion over the Hudson Bay is not significant. The other one is due to the anomalous low-level southerlies that pass over the relatively cool Great Lakes and enhance stability (Holman et al. 2012). Both of them favor a precipitation deficit near Ontario. In the southwest United States, precipitation is increased because of greater moisture flux from the Pacific Ocean and enhanced ascent.

Previous studies generally agree that Atlantic SST has a significant influence on North American precipitation. Our results here are partly consistent with Nigam et al. (2011); both show that, when the TNA SSTs are warmer (cooler) than normal, the eastern United States is drier (wetter) than normal. Whether the tropical Atlantic or North Atlantic is more important is still debated (Enfield et al. 2001; McCabe et al. 2004; Feng et al. 2011; Sutton and Hodson 2005, 2007). In this study, we demonstrate that the tropical Atlantic dominates for large-scale North American precipitation, which agrees with Sutton and Hodson (2007).

5. Summary and discussion

The impacts of global SST modes on North American climate are evaluated comprehensively using the comprehensive statistical method, GEFA, which can separate the impact of a specified SST mode from other oceanic modes. Before applying the GEFA method to observations, it is first validated in the fully coupled climate model CCSM3.5. By comparing results obtained through both statistical (GEFA) and dynamical (ensemble experiments) assessments, it is demonstrated that GEFA can exclusively distinguish the influence of each SST mode on the atmosphere. For North American climate, four observed SST modes are clearly important: ENSO mode, IOB mode, North Pacific EOF1 mode, and tropical Atlantic EOF2 mode. The main conclusions, based on observations, are summarized as follows:

1) The impacts of ENSO on North American climate are qualitatively consistent with previous studies, and in this study these impacts are further quantified. During winter, the warm phase of ENSO can increase the surface air temperature (up to 1.31°C) in southern Canada and the northern United States, decrease the temperature (up to -1.07°C) in the southern United States and Mexico, and increase precipitation in the U.S. Southeast (up to 0.75 mm day^{-1}). During summer, the warm phase of ENSO favors wet (up to 0.59 mm day^{-1}) and cool (up to -0.57°C) conditions in the U.S. Great Plains.
2) It is shown for the first time that the IOB mode can influence surface air temperature across North

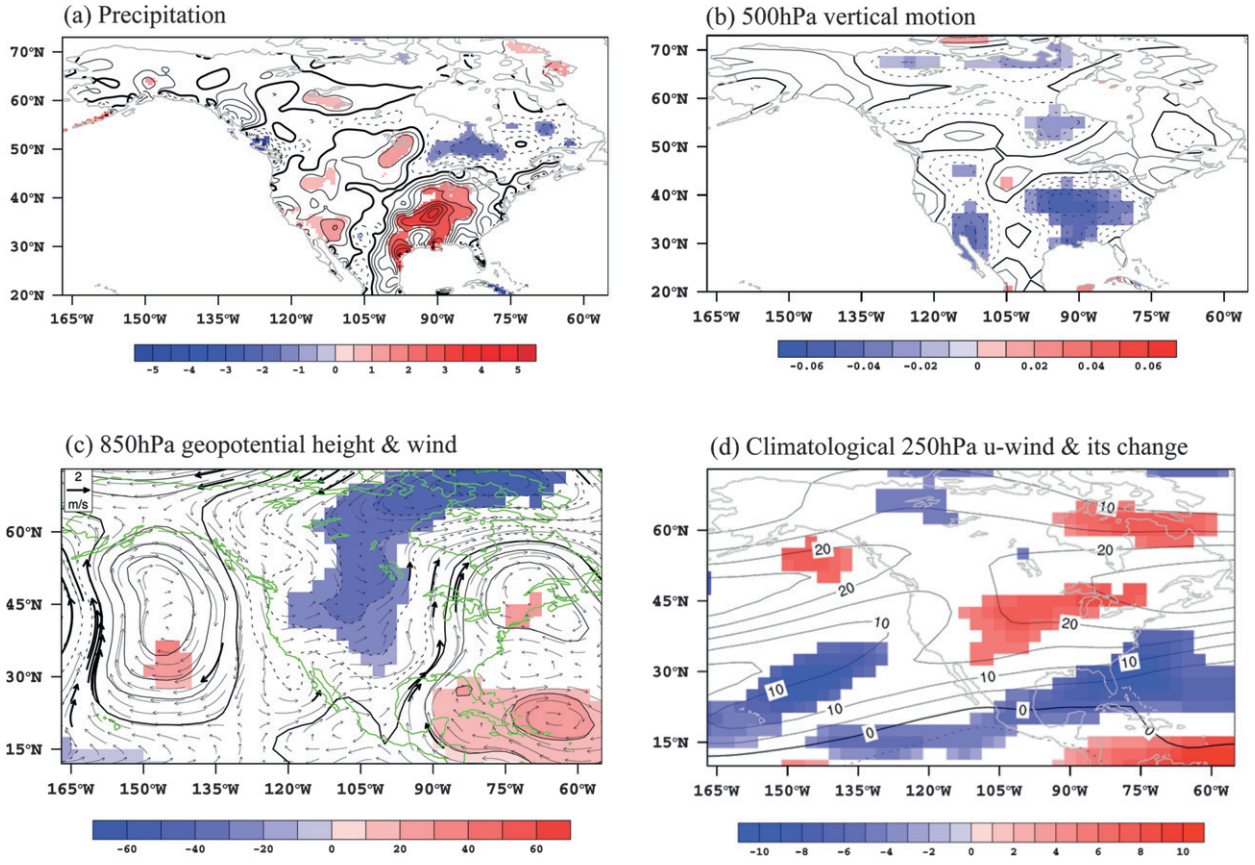

FIG. 9. The response of (a) precipitation (mm day^{-1} °C^{-1}), (b) 500-hPa vertical motion (Pa s^{-1} °C^{-1}; negative means ascending), (c) 850-hPa geopotential height (m °C^{-1}) and wind (m s^{-1} °C^{-1}), and (d) 250-hPa u wind (shading) and climatological u wind (contours; mm s^{-1}) to TA2 forcing (Fig. 2d) during autumn. Shading and thick black arrows indicate ≥90% statistical significance based on Monte Carlo tests.

America even more than ENSO during winter and summer. Previous studies did not find this, likely because they could not separate the impact of IOB from that of ENSO. During both winter and summer, the warm phase of IOB mode tends to produce drying within 40° and 60°N across North America, except for the Pacific Northwest during winter and the Great Plains and Quebec during summer.

3) Our assessment supports the argument that the tropical Atlantic SSTs have more significant influences on North American precipitation than the extratropical North Atlantic SSTs (Sutton and Hodson 2007; Kushnir et al. 2010). The impact is strongest during autumn, with anomalously low (high) tropical North Atlantic SSTs corresponding to wet (dry) conditions across the United States.
4) The influences of NP1 on wintertime surface air temperature and precipitation are somehow different from previous studies by Mantua et al. (1997) and Mantua and Hare (2002). Through the linear combination of ENSO, IOB, and NP1, we can reproduce Mantua's results, indicating that their findings should not be purely attributed to PDO.

Since the GEFA method is a linear statistical method, the response of the atmosphere can be obtained by the linear combination of each mode's impact. For example, during summer, if a cold phase of ENSO coincides with a warm phase of IOB mode, then the northern Great Plains will likely experience a hot, dry summer. However, a warm phase of both ENSO and IOB mode may produce cancelling–opposing impacts on the northern Great Plains, depending on the strength of ENSO and IOB. Therefore, as long as the influences of each individual SST mode are known, the total impacts from these SST modes can be obtained. Conversely, if we know the response of the atmosphere, we can infer which SST modes is the cause. Therefore, seasonal climate prediction for North America will benefit from this study. Since GEFA is a general method, it can be applied over other regions.

Although we have made some progresses, this study has some limitations. The GEFA method is based on linear theory, but in reality SSTs have nonlinear impacts on the atmosphere (Hoerling et al. 1997, 2001). Therefore, our results should be understood as the first-order approximation. Besides SST, there are still other factors that affect the atmosphere, such as land–atmosphere interactions related to vegetation, soil moisture, and snow. In this paper, only SST modes are discussed, while other factors (e.g., vegetation) are discussed in a subsequent paper by Wang et al. (2012, manuscript submitted to *J. Climate*).

Acknowledgments. We thank Drs. Robert Gallimore, Shu Wu, Haijun Yang, Yafang Zhong, and Guangshan Chen for helpful discussions. We also thank three anonymous reviewers for their helpful comments and constructive suggestions. This work is funded by NOAA CPPA and is also partially supported by 2012CB955201, GYHY200906016. Computer resources were provided by DOE NERSC.

REFERENCES

Barlow, M., S. Nigam, and E. H. Berbery, 2001: ENSO, Pacific decadal variability, and U.S. summertime precipitation, drought, and stream flow. *J. Climate,* **14,** 2105–2128.

Collins, W. D., and Coauthors, 2006: The Community Climate System Model version 3 (CCSM3). *J. Climate,* **19,** 2122–2143.

Czaja, A., and C. Frankignoul, 2002: Observed impact of Atlantic SST anomalies on the North Atlantic oscillation. *J. Climate,* **15,** 606–623.

Deser, C., M. A. Alexander, and M. S. Timlin, 2003: Understanding the persistence of sea surface temperature anomalies in midlatitudes. *J. Climate,* **16,** 57–72.

——, A. Capotondi, R. Saravanan, and A. S. Phillips, 2006: Tropical Pacific and Atlantic climate variability in CCSM3. *J. Climate,* **19,** 2451–2481.

Ding, Q. H., B. Wang, J. M. Wallace, and G. Branstator, 2011: Tropical–extratropical teleconnections in boreal summer: Observed interannual variability. *J. Climate,* **24,** 1878–1896.

Eichler, T., and W. Higgins, 2006: Climatology and ENSO-related variability of North American extratropical cyclone activity. *J. Climate,* **19,** 2076–2093.

Enfield, D. B., A. M. Mestas-Nuñez, and P. J. Trimble, 2001: The Atlantic multidecadal oscillation and its relation to rainfall and river flows in the continental U.S. *Geophys. Res. Lett.,* **28,** 2077–2080.

Feng, S., R. J. Oglesby, C. M. Rowe, D. B. Loope, and Q. Hu, 2008: Atlantic and Pacific SST influences on medieval drought in North America simulated by the Community Atmospheric Model. *J. Geophys. Res.,* **113,** D11101, doi:10.1029/2007JD009347.

——, Q. Hu, and R. Oglesby, 2011: Influence of Atlantic sea surface temperatures on persistent drought in North America. *Climate Dyn.,* **37,** 569–586.

Frankignoul, C., and K. Hasselmann, 1977: Stochastic climate models. Part II: Application to sea-surface temperature anomalies and thermocline variability. *Tellus,* **29,** 289–305.

——, and E. K. Kestenare, 2002: The surface heat flux feedback. Part I: Estimates from observations in the Atlantic and the North Pacific. *Climate Dyn.,* **19,** 633–647.

——, A. Czaja, and B. L'Heveder, 1998: Air–sea feedback in the North Atlantic and surface boundary conditions for ocean models. *J. Climate,* **11,** 2310–2324.

Gent, P. R., S. G. Yeager, R. B. Neale, S. Levis, and D. A. Bailey, 2010: Improvements in a half degree atmosphere/land version of the CCSM. *Climate Dyn.,* **34,** 819–833.

Gill, A. E., 1980: Some simple solutions for heat-induced tropical circulation. *Quart. J. Roy. Meteor. Soc.,* **106,** 447–462.

Guan, B., and S. Nigam, 2009: Analysis of Atlantic SST variability factoring interbasin links and the secular trend: Clarified structure of the Atlantic multidecadal oscillation. *J. Climate,* **22,** 4228–4240.

Halpert, M. S., and C. F. Ropelewski, 1992: Surface temperature patterns associated with the Southern Oscillation. *J. Climate,* **5,** 577–593.

Hasselmann, K., 1976: Stochastic climate models. Part I: Theory. *Tellus,* **28,** 473–485.

Hoerling, M. P., and A. Kumar, 2003: The perfect ocean for drought. *Science,* **299,** 691–694.

——, ——, and M. Zhong, 1997: El Niño, La Niña, and the nonlinearity of their teleconnections. *J. Climate,* **10,** 1769–1786.

——, ——, and T. Xu, 2001: Robustness of the nonlinear climate response to ENSO's extreme phases. *J. Climate,* **14,** 1277–1293.

Holman, K. D., A. Gronewold, M. Notaro, and A. Zarrin, 2012: Improving historical precipitation estimates over the Lake Superior basin. *Geophys. Res. Lett.,* **39,** L03405, doi:10.1029/2011GL050468.

Holton, J. R., 1979: *An Introduction to Dynamic Meteorology*. 2nd ed. International Geophysics Series, Vol. 23, Academic Press, 391 pp.

Honda, M., S. Yamane, and H. Nakamura, 2005: Impacts of the Aleutian–Icelandic low seesaw on surface climate during the twentieth century. *J. Climate,* **18,** 2793–2802.

Hoskins, B. J., and D. J. Karoly, 1981: The steady linear response of a spherical atmosphere to thermal and orographic forcing. *J. Atmos. Sci.,* **38,** 1179–1196.

Hu, Z.-Z., and B. Huang, 2009: Interferential impact of ENSO and PDO on dry and wet conditions in the U.S. Great Plains. *J. Climate,* **22,** 6047–6065.

Kalnay, E., Coauthors, 1996: The NCEP/NCAR 40-Year Reanalysis Project. *Bull. Amer. Meteor. Soc.,* **77,** 437–471.

Kiladis, G. N., and H. F. Diaz, 1989: Global climatic anomalies associated with extremes in the Southern Oscillation. *J. Climate,* **2,** 1069–1090.

Kushnir, Y., R. Seager, M. Ting, N. Naik, and J. Nakamura, 2010: Mechanisms of tropical Atlantic SST influence on North American precipitation variability. *J. Climate,* **23,** 5610–5628.

Lin, S. J., 2004: A ''vertically Lagrangian'' finite-volume dynamical core for global models. *Mon. Wea. Rev.,* **132,** 2293–2307.

Liu, Z., and L. Wu, 2004: Atmospheric response to North Pacific SST: The role of ocean–atmosphere coupling. *J. Climate,* **17,** 1859–1882.

——, and N. Wen, 2008: On the assessment of nonlocal climate feedback. Part II: EFA-SVD and optimal feedback modes. *J. Climate,* **21,** 5402–5416.

——, M. Notaro, J. Kutzbach, and N. Liu, 2006: Assessing global vegetation–climate feedbacks from observations. *J. Climate,* **19,** 787–814.

——, N. Wen, and Y. Liu, 2008: On the assessment of nonlocal climate feedback. Part I: The generalized equilibrium feedback assessment. *J. Climate,* **21,** 134–148.

——, ——, and L. Fan, 2012a: Assessing atmospheric response to surface forcing in the observations. Part I: Cross-validation of annual response using GEFA, LIM, and FDT. *J. Climate,* **25,** 6796–6816.

——, L. Fan, S.-I. Shin, and Q. Liu, 2012b: Assessing atmospheric response to surface forcing in the observations. Part II: Cross-validation of seasonal response using GEFA and LIM. *J. Climate,* **25,** 6817–6834.

Mantua, N. J., and S. R. Hare, 2002: The Pacific decadal oscillation. *J. Oceanogr.,* **58,** 35–44.

——, ——, Y. Zhang, J. M. Wallace, and R. C. Francis, 1997: A Pacific interdecadal climate oscillation with impacts on salmon production. *Bull. Amer. Meteor. Soc.,* **78,** 1069–1079.

McCabe, G. J., M. A. Palecki, and J. L. Betancourt, 2004: Pacific and Atlantic Ocean influences on multidecadal drought frequency in the United States. *Proc. Natl. Acad. Sci. USA,* **101,** 4136–4141.

Neale, R. B., J. H. Richter, and M. Jochum, 2008: The impact of convection on ENSO: From a delayed oscillator to a series of events. *J. Climate,* **21,** 5904–5924.

Neelin, J. D., 2011: *Climate Change and Climate Modeling*. Cambridge University Press, 304 pp.

Nigam, S., B. Guan, and A. Ruiz-Barradas, 2011: Key role of the Atlantic multidecadal oscillation in 20th century drought and wet periods over the Great Plains. *Geophys. Res. Lett.,* **38,** L16713 doi:10.1029/2011GL048650.

Notaro, M., and Z. Y. Liu, 2008: Statistical and dynamical assessment of vegetation feedbacks on climate over the boreal forest. *Climate Dyn.,* **31,** 691–712.

——, Z. Liu, and J. W. Williams, 2006: Observed vegetation–climate feedbacks in the United States. *J. Climate,* **19,** 763–786.

——, Y. Wang, Z. Liu, R. Gallimore, and S. Levis, 2008: Combined statistical and dynamical assessment of simulated vegetation-rainfall during the mid-Holocene. *Global Change Biol.,* **14,** 347–368.

Peng, S., and J. S. Whitaker, 1999: Mechanisms determining the atmospheric response to midlatitude SST anomalies. *J. Climate,* **12,** 1393–1408.

——, L. A. Mysak, J. Derome, H. Ritchie, and B. Dugas, 1995: The differences between early and midwinter atmospheric responses to sea surface temperature anomalies in the northwest Atlantic. *J. Climate,* **8,** 137–157.

Rayner, N. A., D. E. Parker, E. B. Horton, C. K. Folland, L. V. Alexander, D. P. Rowell, E. C. Kent, and A. Kaplan, 2003: Global analyses of sea surface temperature, sea ice, and night marine air temperature since the late nineteenth century. *J. Geophys. Res.,* **108,** 4407, doi:10.1029/2002JD002670.

Rogers, J. C., and J. S. M. Coleman, 2003: Interactions between the Atlantic multidecadal oscillation, El Niño/La Niña, and the PNA in winter Mississippi valley stream flow. *Geophys. Res. Lett.,* **30,** 1518, doi:10.1029/2003GL017216.

Ropelewski, C. F., and M. S. Halpert, 1986: North American precipitation and temperature patterns associated with the El Niño/Southern Oscillation (ENSO). *Mon. Wea. Rev.,* **114,** 2352–2362.

——, and ——, 1987: Global and regional scale precipitation patterns associated with the El Niño/Southern Oscillation. *Mon. Wea. Rev.,* **115,** 1606–1626.

——, and ——, 1989: Precipitation patterns associated with the high index phase of the Southern Oscillation. *J. Climate,* **2,** 268–284.

Schneider, N., and B. D. Cornuelle, 2005: The forcing of the Pacific decadal oscillation. *J. Climate,* **18,** 4355–4373.

Schubert, S. D., M. J. Suarez, P. J. Pegion, R. D. Koster, and J. T. Bacmeister, 2004: On the cause of the 1930s dust bowl. *Science,* **303,** 1855–1859.

Seager, R., N. Harnik, W. A. Robinson, Y. Kushnir, M. Ting, H. P. Huang, and J. Velez, 2005a: Mechanisms of ENSO-forcing of hemispherically symmetric precipitation variability. *Quart. J. Roy. Meteor. Soc.,* **131,** 1501–1527.

——, Y. Kushnir, C. Herweijer, N. Naik, and J. Velez, 2005b: Modeling of tropical forcing of persistent droughts and pluvials over western North America: 1856–2000. *J. Climate,* **18,** 4065–4088.

Sun, S., and G. Wang, 2012: The complexity of using a feedback parameter to quantify the soil moisture-precipitation relationship. *J. Geophys. Res.,* **117,** D11113, doi:10.1029/2011JD017173.

Sutton, R. T., and D. L. R. Hodson, 2005: Atlantic Ocean forcing of North American and European summer climate. *Science,* **309,** 115–118.

——, and ——, 2007: Climate response to basin-scale warming and cooling of the North Atlantic Ocean. *J. Climate,* **20,** 891–907.

Ting, M., and H. Wang, 1997: Summertime U.S. precipitation variability and its relation to Pacific sea surface temperature. *J. Climate,* **10,** 1853–1873.

Trenberth, K. E., and C. J. Guillemot, 1996: Physical processes involved in the 1988 drought and 1993 floods in North America. *J. Climate,* **9,** 1288–1298.

——, G. W. Branstator, and P. A. Arkin, 1988: Origins of the 1988 North American drought. *Science,* **242,** 1640–1645.

Webster, P. J., and J. Fasullo, 2003: Dynamic theory of monsoons. *Encyclopedia of Atmospheric Sciences,* J. R. Holton, J. A. Curry, and J. A. Pyle, Eds., Academic Press, 1370–1386.

Wen, N., Z. Y. Liu, Q. Y. Liu, and C. Frankignoul, 2010: Observed atmospheric responses to global SST variability modes: A unified assessment using GEFA. *J. Climate,* **23,** 1739–1759.

Willmott, C. J., and K. Matsuura, 1995: Smart interpolation of annually averaged air temperature in the United States. *J. Appl. Meteor.,* **34,** 2577–2586.

Wu, R. G., and J. L. Kinter, 2009: Analysis of the relationship of U.S. droughts with SST and soil moisture: Distinguishing the time scale of droughts. *J. Climate,* **22,** 4520–4538.

Yang, J., Q. Liu, S.-P. Xie, Z. Liu, and L. Wu, 2007: Impact of the Indian Ocean SST basin mode on the Asian summer monsoon. *Geophys. Res. Lett.,* **34,** L02708, doi:10.1029/2006GL028571.

——, ——, Z. Liu, L. Wu, and F. Huang, 2009: Basin mode of Indian Ocean sea surface temperature and Northern Hemisphere circumglobal teleconnection. *Geophys. Res. Lett.,* **36,** L19705, doi:10.1029/2009GL039559.

Zhang, T., M. P. Hoerling, J. Perlwitz, D.-Z. Sun, and D. Murray, 2011: Physics of U.S. surface temperature response to ENSO. *J. Climate,* **24,** 4874–4887.

Zhong, Y. F., Z. Y. Liu, and M. Notaro, 2011: A GEFA assessment of observed global ocean influence on U.S. precipitation variability: Attribution to regional SST variability modes. *J. Climate,* **24,** 693–707.